



Cite this: *Phys. Chem. Chem. Phys.*,
2015, 17, 26036

Received 19th July 2015,
Accepted 8th September 2015

DOI: 10.1039/c5cp04222d

www.rsc.org/pccp

Glitter in a 2D monolayer†

Li-Ming Yang,*^a Matthew Dornfeld,^b Thomas Frauenheim^a and Eric Ganz^b

We predict a highly stable and robust atomically thin gold monolayer with a hexagonal close packed lattice stabilized by metallic bonding with contributions from strong relativistic effects and aurophilic interactions. We have shown that the framework of the Au monolayer can survive 10 ps MD annealing simulations up to 1400 K. The framework is also able to survive large motions out of the plane. Due to the smaller number of bonds per atom in the 2D layer compared to the 3D bulk we observe significantly enhanced energy per bond (0.94 vs. 0.52 eV per bond). This is similar to the increase in bond strength going from 3D diamond to 2D graphene. It is a non-magnetic metal, and was found to be the global minima in the 2D space. Phonon dispersion calculations demonstrate high kinetic stability with no negative modes. This 2D gold monolayer corresponds to the top monolayer of the bulk Au(111) face-centered cubic lattice. The close-packed lattice maximizes the aurophilic interactions. We find that the electrons are completely delocalized in the plane and behave as 2D nearly free electron gas. We hope that the present work can inspire the experimental fabrication of novel free standing 2D metal systems.

I. Introduction

Gold has been playing a special role in human society throughout history. This unique role is closely related to its unusual resistance to oxidation, and also its exceptional stability during chemical reactions, extreme pressures, and elevated temperatures.¹ The exceptional stability of bulk gold is mainly ascribed to its strong relativistic effect² and the so-called aurophilic attractions.³ As one of the noblest of all metals, unlike other transition metal catalysts, gold had long been viewed as catalytically inactive. While bulk gold is known as the most chemically inert metal in the periodic table, nanometer-sized gold particles are exceptionally

active as catalysts in a wide range of chemical transformations.⁴ It has been shown that the catalytic properties of gold nanoparticles are sensitive to many factors, including the nature of the substrate, and the size, shape, and charge state of the gold particles.^{4,5} Furthermore, some intriguing and surprising structural motifs have been discovered for gold clusters, such as planar structures up to Au_{12}^- ,⁶ the hollow golden cage Au_n^- ($n = 16-18$),⁷ the golden pyramid Au_{20}^- ,⁸ and the non-icosahedral low-symmetry Au_{55}^- .⁹ Considering the dramatic and surprising differences in gold chemistry between the bulk and nanoscale phases, one can see that the quantum effects, dimensionality effects, and size and shape effects are especially significant for gold. Furthermore, novel forms of gold nanostructures, including helical multi-shell gold nanowires,¹⁰ and helical single walled gold nanotubes¹¹ have been fabricated experimentally.

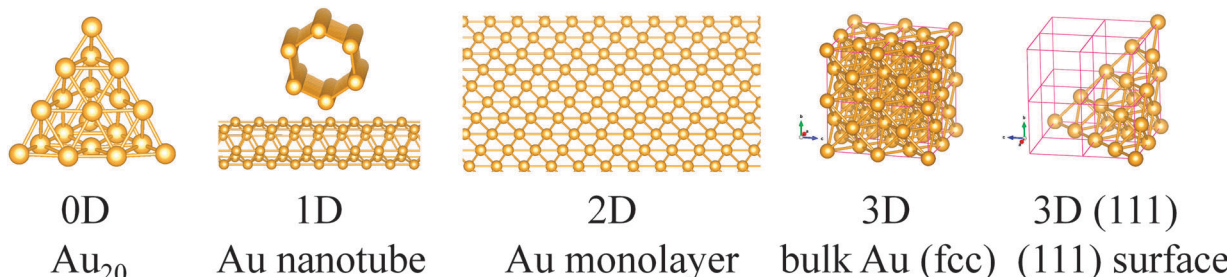
In an exciting recent development, free-standing atomically thick iron membranes suspended in graphene pores have been fabricated experimentally.¹² These iron layers were small with just up to 10 atoms wide inside the pores. These iron patches had a different structure than the predicted full 2D isolated layer. This demonstrates the potential of perforated graphene as a support for small 2D membranes, and paves the way for novel 2D structures to be formed. Zhao *et al.* also used density functional theory (DFT) calculations to study these systems, and predicted that the largest thermodynamically stable patch would be 12 atoms across.¹² This method could potentially be used to fabricate a small free-standing Au monolayer. Koskinen and Korhonen have studied the solid and liquid phases of a small monolayer gold patch in a graphene hole (using density functional tight binding, and also DFT).¹³ This 49 atom gold patch stayed solid up to 700 K, and then at 900 K formed an unusual 2D liquid layer.

As we know, dimensionality is one of the most important parameters that influence material properties. The same chemical compounds can exhibit dramatically different properties depending on whether they are arranged in 0D, 1D, 2D, or 3D crystal structures. This is clearly demonstrated by the different carbon allotropes, including fullerenes (0D),¹⁴ nanotubes (1D),¹⁵ graphene (2D),¹⁶

^a Bremen Center for Computational Materials Science, University of Bremen,
Am Fallturm 1, Bremen, 28359, Germany. E-mail: lmyang.uio@gmail.com

^b Department of Physics, University of Minnesota, 116 Church St. SE, Minneapolis,
Minnesota 55416, USA

† Dedicated to Prof. Jack Simons on the occasion of his 70th birthday.



Scheme 1 We follow the evolution of gold structures from 0D Au_{20} clusters to 1D gold nanowires and nanotubes to the 2D gold monolayer. We then continue to the 3D bulk gold fcc structure. Note that many of these elements contain the (111) surface in common.

and diamond (3D). These carbon allotrope materials have a huge impact on modern nanoscience and technology. Below, we will see a similar progression for gold materials.

The relationships between the different gold allotropes can be established from a topological perspective. We follow the changes in structure and properties of the gold materials as we go from clusters to nanoparticles to 1D nanotubes or nanowires to the 2D layer, to the 3D bulk phase (see Scheme 1). We note that the $\text{Au}(111)$ bulk surface is also widely used as a substrate for adsorption and surface science studies.¹⁷ Each of the four faces of Au_{20} is a (111) surface. Conceptually, Au nanotubes can be created by rolling a section of the Au monolayer into a seamless cylinder. Similar to carbon nanotubes,¹⁸ gold nanotubes can also be indexed by a pair of integers (n, m). Depending on the values of n and m , the nanotubes may be zigzag, armchair, or chiral. Also, the Au monolayer consists of a single layer of the $\text{Au}(111)$ surface.

This free-standing Au 2D monolayer sheet could potentially be used as a substrate for the adsorption of small molecules (or biological molecules) for analysis in an electron microscope. Furthermore, functional groups could be added to the surface to modify or improve the electronic properties, optical properties, and potentially even catalytic activity.

In this work, we study the free-standing two-dimensional monolayer gold. A free-standing gold monolayer has not been fabricated or reported experimentally to date. We hope that these results will inspire experimental fabrication of novel free-standing 2D metal layers. It is important to elucidate the unusual structure, chemistry, and intriguing physics of these new 2D materials.

II. Computational methodology

First-principles calculations were performed using density functional theory with the generalized gradient approximation (GGA) with the Perdew–Burke–Ernzerhof (PBE)¹⁹ exchange–correlation functional. We used the projected augmented wave (PAW)²⁰ pseudopotential for Au with a plane wave cutoff energy of 500 eV as implemented in the VASP code.²¹ It is well known that the relativistic effect can be divided into three terms: the mass-velocity correction, the Darwin term, and the spin–orbit (SO) coupling term, in which the first two terms are called the scalar relativistic (SR) effect. Usually, the SR is much larger than

the SO and plays a decisive role in determining the correct geometrical structures of the ground state of gold materials.²² Following commonly used methods in the community, crystal structures were optimized at the scalar-relativistic (SR) level, and the single point energy calculations were performed at the spin-orbit (SO) level. The positions of atoms, lattice parameters, and angles were fully optimized using the conjugate gradient (CG) method. Therefore, the maximum force acting on each atom is less than 10^{-3} eV Å⁻¹. The criterion for energy convergence is 10^{-6} eV per cell. We put the monolayer Au sheet on the xy plane with the z -direction perpendicular to the layer plane. A vacuum space of 16 Å in the z -direction was used to avoid interactions between the adjacent layers. The Brillouin zone was sampled with a $21 \times 21 \times 1$ Γ -centered Monkhorst–Pack (MP)²³ K -points grid (sampling resolution $2\pi \times 0.02$). Lattice dynamics were evaluated using the finite displacement method²⁴ implemented in the CASTEP package²⁵ in Materials Studio 7.0. This was done at the “ultrafine” level within the local-density approximation (LDA) CA-PZ using ultrasoft pseudopotentials. The energy cutoff was set at 440 eV and the SCF tolerance was set at 5×10^{-7} eV per atom. The Brillouin zone was sampled with a $21 \times 21 \times 1$ MP grid for both phonon dispersion and phonon density of states. The supercell defined by the cutoff radius was set at 9.0 Å for the finite displacement method. The supercell volume will be 25 times that of the normal cell. The separation of dispersion in the Brillouin zone was set at 0.003 Å⁻¹, which represents the average distance between Monkhorst–Pack mesh q -points used in the real space dynamical matrix calculations.

Ab initio Born–Oppenheimer molecular dynamics (BOMD) simulations were performed to assess the thermal stability of the Au monolayer. The scalar-relativistic DFT-D method and the Tkatchenko–Scheffler (TS) method were used in CASTEP²⁵ in Materials Studio 7.0. MD simulation in an NVT ensemble was carried out for 10 ps with a time step of 1.0 fs (parameters: accuracy fine, SCF = 3×10^{-6} , smearing = 0.04, DIIS = 20, Nosé–Hoover,²⁶ Nosé Q = 2, Nosé chain length = 2). We fixed the center of mass for 1338–1600 K simulations. Materials Studio was also used to create the initial structures and visualize the results. Root Mean Square Deviation (RMSD) was calculated using the differences between the nearest neighbor bond lengths and the 0 K optimized bond length. We feel that it is important to include the dispersion interactions in the calculations

due to the long bond length extensions encountered at elevated temperatures.

The crystal structure predictions were performed with evolutionary algorithm as implemented in the USPEX code.²⁷ In these calculations, initial structures are randomly produced using planar group symmetry. All newly produced structures are relaxed and the relaxed energies are used for selecting structures as parents of the new generation of structures (produced by carefully designed variation operators, such as heredity and soft mutation). In these calculations, we considered systems with up to 18 atoms in the unit cell, and used 30 structures in each generation, with 60% of the lowest-enthalpy structures allowed to produce the next generation through heredity (60%), lattice mutation (30%), and atomic permutation (10%); in addition, two lowest-enthalpy structures were allowed to survive into the next generation. The structure relaxations during the evolutionary algorithm were performed using the PBE functional as implemented in VASP. The VESTA software²⁸ was used for visualization and plot.

III. Results and discussion

In this section, we will discuss the stability and viability of the predicted free-standing Au monolayer through several evaluation methods. These include the thermodynamic stability *via* comprehensive structure search and cohesive energy evaluation, kinetic stability by phonon dispersion calculation, thermal stability and viability at elevated temperature from molecular dynamics simulations. Then, we reveal the unique chemical bonding in the gold monolayer using the electron localization function, electronic properties, and mechanical properties.

A. Stability and viability of the Au monolayer

A.1. Crystal structure search. The ground state structure of the Au monolayer was obtained using a comprehensive evolutionary algorithm structural search with USPEX,²⁷ followed by the full relaxation of random structures with VASP²¹ (see details in Section II). The structural search predicts that the global minimum structure of the free-standing Au monolayer is a hexagonally close packed (HCP) sheet (Fig. 1a), which will become a new member in the planar hypercoordinate flatland.²⁹ Other motifs, such as Fig. 1b square, Fig. 1c honeycomb, and Fig. 1d tetracoordinate have relative energies of +299 [313], +647 [652], +757 [788] meV per atom respectively at the

SR [SR + SO] level. All these have significantly higher energies than the HCP ground state. We then performed an analysis of properties including chemical bonding, cohesive energy, mechanical properties, dynamic stability, thermal stability, and electronic properties.

We have considered various structures of 2D Au including both planar and buckled. The buckled structure of Au automatically transforms to the exactly planar motif during geometry optimization. The space group of the Au monolayer is *P6/mmm* (#191). One unit cell of the Au monolayer consists of one Au atom, the optimized lattice constants of $a = b = 2.755 \text{ \AA}$. The calculated Au–Au bond lengths are 2.755 \AA . Therefore, the hexagonal close packed Au monolayer is the global minimum structure in the 2D space. Furthermore, the closely packed motifs with a maximum of Au–Au bonds, and evenly distributed coordination in the 2D plane can maximize the stability of this 2D monolayer sheet. This is consistent with and further evidence the fact that the chemistry of gold is dominated by its strong relativistic effect² and the so-called aurophilic attractions.³ The gold monolayer sheet predicted to be the global minimum is very exciting and it holds great potential to be realized experimentally.

A.2. Cohesive energy of the 2D Au monolayer. To evaluate the stability of this structure, we first computed the cohesive energies $E_{\text{coh,monolayer}} = (mE_{\text{Au-atom}} - E_{\text{Au-monolayer}})/m$, and $E_{\text{coh,bulk}} = (mE_{\text{Au-atom}} - E_{\text{Au-bulk}})/m$. With $E_{\text{Au-atom}}$, $E_{\text{Au-monolayer}}$, and $E_{\text{Au-bulk}}$ being the total energies of a single Au atom, one unit cell of the Au monolayer and one unit cell of bulk gold in face-centered cubic (fcc) phase, respectively. The Au monolayer has a cohesive energy of 2.71 [2.82] at the SR [SR + SO] levels, respectively. The Au bulk has a cohesive energy of 2.98 [3.11] eV per atom respectively. One can see that the spin-orbit (SO) interaction has a small effect on the cohesive energy. This is consistent with the previous studies on the effects of spin-orbit (SO) interaction on gold chemistry. Although the cohesive energy of the 2D Au monolayer is a bit smaller than that of the 3D bulk fcc phase, it is still important to consider the lower number of bonds per atom (6 vs. 12, respectively). Therefore each bond is stronger in the sheet than in the bulk (0.94 eV per bond vs. 0.52 eV per bond, respectively). The framework of the 2D Au monolayer is stabilized by the closely packed hexacoordinate lattice, which forms the maximum number of chemical bonds within the plane. The close packed configuration can form an alliance of chemical bonds, which further strengthen and stabilize this 2D sheet.

A.3. Phonon dispersion of the 2D Au monolayer. The necessary and sufficient condition for dynamical stability of a

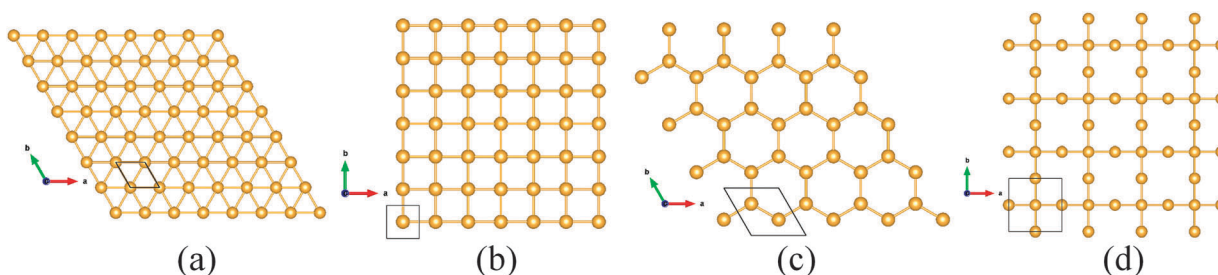


Fig. 1 Different motifs of the 2D Au-monolayer: (a) hexagonal close packed, (b) square, (c) honeycomb, and (d) tetracoordinate.

crystal at low temperature is phonon stability. The dynamical stability of the Au monolayer was tested by calculating the phonon dispersion along the high-symmetry lines $\Gamma-K-M-\Gamma$ (Fig. 2). The absence of soft modes within the entire Brillouin zone clearly indicates that the Au monolayer is minimum on the potential energy surface. All the frequencies are real, demonstrating good kinetic stability. The highest frequency reaches up to 220 cm^{-1} , indicating a robust Au–Au interaction.

A.4. Molecular dynamics simulation of the 2D Au monolayer. To verify that this new material will be stable under ambient conditions, we have performed *ab initio* molecular dynamics simulations over a range of temperatures. A 5×6 supercell was used under periodic boundary conditions. A series of individual MD simulations were carried out to evaluate the thermal stability of the materials. For the Au monolayer, simulations were run at 500, 800, 1200, 1338, 1400, 1600, and 2000 K. The simulations extended to times up to 10 ps for most simulations, and up to 18 ps at 1338 K. Note that the melting point of bulk Au is 1338 K. Ignoring the first ps as a warm up period, the framework was maintained up to 1400 K for 10 ps, but melted by 1600 K after 4 ps, completely melted at 2000 K after 1 ps. Bond length extensions of 14%, 17%, 21%, 36%, and 43% were observed for

500, 800, 1200, 1338, and 1400 K simulations respectively. RMSD values of 0.10, 0.15, and 0.12 were calculated for 500, 800, and 1200 K. Snapshots taken at the end of each simulation are shown in Fig. 3. At 1600 K, we observe holes in the 2D layer, left behind by atoms that have moved on top of the layer. Note that Koskinen and Korhonen have observed interesting 2D liquid behavior under periodic boundary conditions in a 8×8 unit cell by DFT molecular dynamics simulation of this system at 1600 K.¹³ We have also confirmed this behavior using an 8×8 cell, and will discuss these results in a future paper.

B. Electronic structures of the Au monolayer

To get insight into electronic properties, we have computed the band structure as well as its density of states (DOS). As shown in Fig. 4, the material shows a band structure typical of metals. The metallic character of the Au monolayer is demonstrated by the Fermi level ($E = 0$) located inside the bands, and no band gap was observed at this energy. We see that a nearly-free electron like band meets the Fermi level halfway up, indicating that the valence electrons have been donated into the nearly-free electron gas (between the Γ point and the K point, similar to the bulk). Therefore, similar to the bulk, the Au monolayer is a diamagnetic metal.

The partial density of states (PDOS) analysis shows that below the Fermi energy the major contribution comes from Au 5d-states. Whereas the states at the Fermi level are dominated by the 6p-, 5d-, 6s-states, with Au-6p being larger than Au-5d and Au-6s. There is apparent hybridization between Au 5d- and 6s-states. This is consistent with the relativistic stabilization of its outer 6s orbital. The relativistic effects also lead to destabilization of the 5d orbitals, reducing the 6s-5d energy gap and enhancing s-d hybridization. We observe a sharp peak at 2.1 eV below the Fermi level.

The band structure indicates that these materials are metallic with a large density-of-states (DOS) at the Fermi level. The Au monolayer is diamagnetic as confirmed by a spin-polarized computation, indicating that the compound has a nonmagnetic ground state. Solid State Adaptive Natural Density Partitioning (SSAdNDP) was used to search for localized bonding.³⁰ No localized bonding was observed. The bonding is completely delocalized, similar to 3D metals. The predicted gold monolayer is a metal. The bonding situation is in sharp contrast to

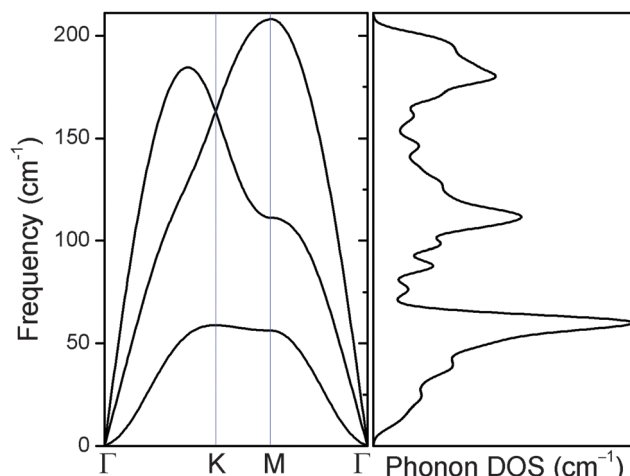


Fig. 2 Phonon dispersion and phonon density of states of the Au monolayer. Γ (0, 0, 0), M (0, 1/2, 0), K (1/3, 2/3, 0) refer to special points in the first Brillouin zone in reciprocal space.

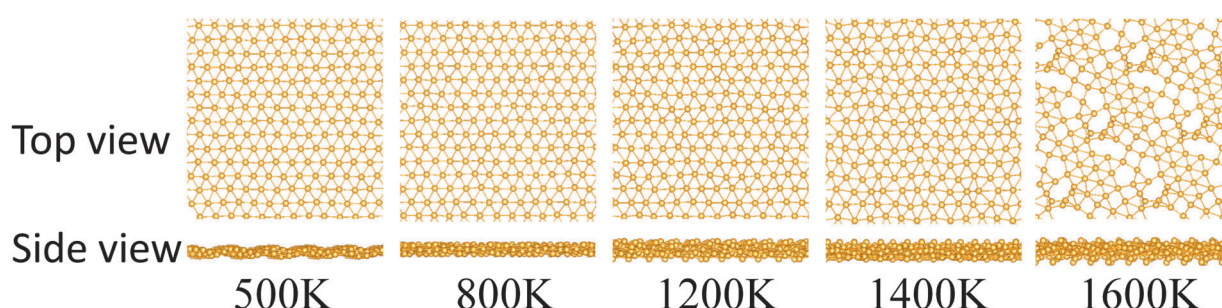


Fig. 3 Snapshots of the final frame of each molecular dynamics simulation from the Au monolayer at 500, 800, 1200, 1400, and 1600 K (top and side views).

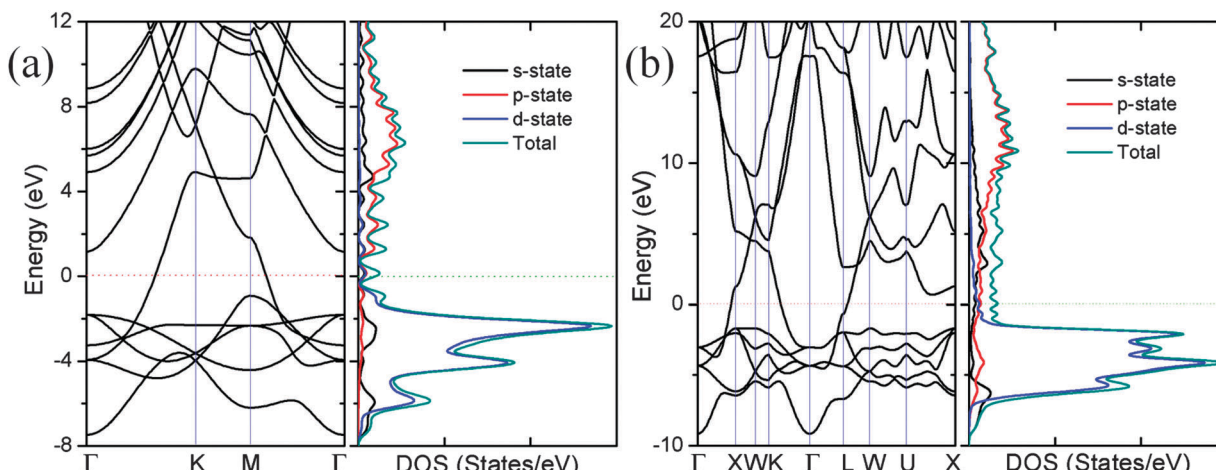


Fig. 4 Electronic structures of 2D Au monolayer (a) and 3D bulk Au (b). Band structure (left), total density of states (TDOS) and partial density of states (PDOS) (right) are shown. The Fermi level is at 0 eV.

that of the isolated gold clusters, which were revealed to have 4c–2e bonds *via* SSAdNDP analysis.³¹ Therefore, we see that the dimensionality and quantum confinement have profound effects on the chemical bonding of gold systems.

C. Chemical bonding analyses

C.1. Electron localization function. The electron localization function (ELF) provides a good description of electron delocalization in molecules³² and solids³³ and is a useful tool for chemical bond classification.³⁴ We calculated the ELF of the Au monolayer to identify its delocalization character. As a comparison, we also consider the ELF of the bulk gold fcc

phase. Slices parallel to the (111) crystal face of bulk gold fcc phase crossing the hexagonal close packed atoms together with the ELF of the 2D Au monolayer are plotted in Fig. 5. One can see that the ELF values for the Au monolayer are very low, similar to bulk Au(111), delocalization in the whole sheet is evident.

C.2. Charge density. The electron charge density distribution provides detailed and useful information on the chemical bonding. Fig. 6 shows the charge density of the 2D Au monolayer compared to the charge density of 3D bulk gold. We see that these charge density distributions are essentially the same. Valence electrons from the monolayer have delocalized into the whole 2D sheet forming a nearly free electron gas.

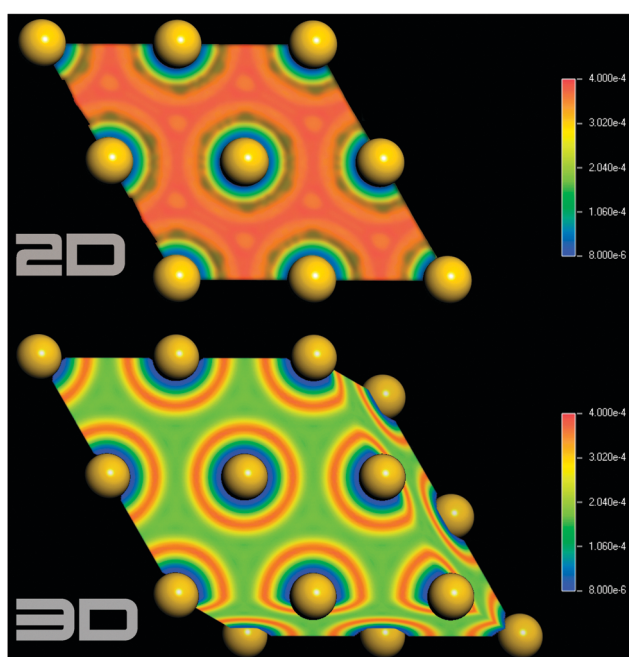


Fig. 5 Color plot of ELF for the 2D Au monolayer (upper panel) and 3D bulk gold (lower panel).

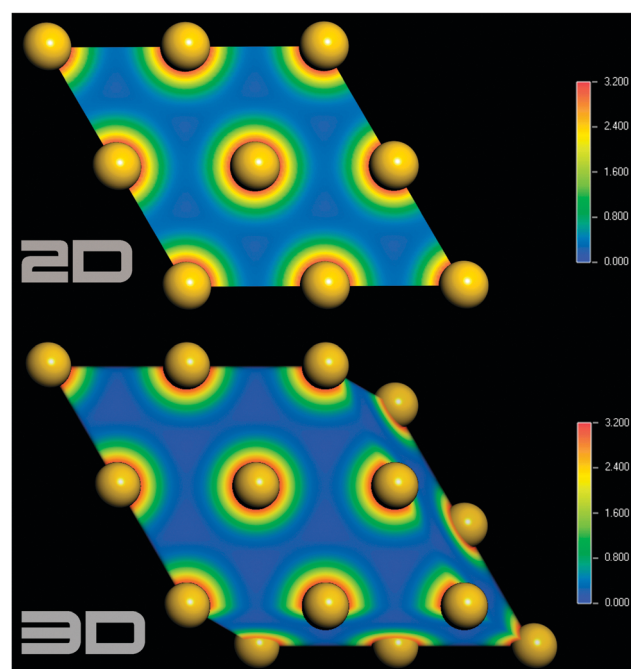


Fig. 6 Color image of the electron charge density of the 2D Au monolayer (upper panel) and 3D bulk Au (lower panel).

D. Mechanical properties

Bulk gold is a malleable and ductile metal and has wide application in electronic engineering, mechanical engineering, electronic devices, etc. Below, we probe the mechanical properties of the Au monolayer. The mechanical properties are important for potential application of the Au monolayer material. The gold monolayer has three independent elastic constants: c_{11} , c_{12} , and c_{44} . Our calculations generate $c_{11} = 52.9$ GPa, $c_{12} = 30.6$ GPa, and $c_{44} = 11.1$ GPa, which follow a correlation of $c_{11} = c_{12}$, $c_{44} = (c_{11} - c_{12})/2$. The Au monolayer shows very good elastic properties and can be rolled into nanotubes (see Scheme 1). Indeed, a single-walled gold nanotube (SWGT) was experimentally found using a UHV electron microscope at 150 K by Oshima *et al.*, which was considered as a (5,3) SGBT composed of five atomic rows coiling around the tube axis.¹¹

The in-plane Young modulus (or in-plane stiffness) is commonly used to evaluate the mechanical stability of 2D materials. We compare the calculated value of our new material to previous theoretical results³⁵ for several commonly known 2D materials, including silicene and germanene. For the Au monolayer, the in-plane stiffness was computed to be 56 N m⁻¹. This value is significantly higher than our predicted result for a free-standing 2D Ag layer with 31 N m⁻¹.³⁶ This is also higher than germanene (42 N m⁻¹), and comparable to silicene (61 N m⁻¹) computed at the same theoretical levels. Thus, the Au monolayer shows good mechanical stability.

IV. Conclusions

In summary, we have comprehensively explored the freestanding 2D Au monolayer sheet. Molecular dynamics simulations show that the Au monolayer is stable during short 10 ps annealing runs up to 1400 K. The framework is able to survive large motions out of the plane. Due to the smaller number of bonds per atom in the 2D layer compared to the 3D bulk we observe significantly enhanced energy per bond (0.94 vs. 0.52 eV per bond). This is similar to the increase in bond strength going from 3D diamond to 2D graphene. It is a nonmagnetic metal. Some of the electrons are delocalized over the whole sheet and form a nearly free 2D electron gas. The Au monolayer has a planar hexacoordinated gold configuration. The metallic bonds hold the gold atoms together in the 2D plane. The Au-Au interactions were strengthened and maximized by strong relativistic effects and auophilic attractions. Local structural stability is predicted by the absence of any imaginary phonon modes. An evolutionary algorithm search confirmed that the Au monolayer is the global minimum structure in the 2D space. Considering the rapid development of experimental techniques for fabrication of low-dimensional materials in recent years, we are optimistic that the freestanding 2D Au monolayer can be fabricated experimentally in the near future. Our results provide new insights into possible applications of Au systems. We hope these results inspire fabrication and study of novel 2D metal and alloy systems.

Acknowledgements

Support in Germany by Fellowship of Hanse-Wissenschaftskolleg (HWK) and Research Scholarship of University of Bremen (to L.-M.Y) are gratefully acknowledged. We thank the Minnesota supercomputer Institute, HLRN & JULICH supercomputers for support.

References

- (a) T. Green, *The New World of Gold: The Inside Story of the Mines, the Markets, the Politics, the Investors*, Walker & Company, New York, 1984, p. 324; (b) P. Bernstein, *The Power of Gold: The History of an Obsession*, Wiley, New York, 2001, p. 448;
- (c) B. Hammer and J. K. Norskov, *Nature*, 1995, **376**, 238;
- (d) D. Batani, A. Balducci, D. Beretta, A. Bernardinello, T. Löwer, M. Koenig, A. Benazzi, B. Faral and T. Hall, *Phys. Rev. B: Condens. Matter Mater. Phys.*, 2000, **61**, 9287.
- 2 P. Pykko, *Chem. Rev.*, 1988, **88**, 563.
- 3 F. Scherbaum, A. Grohmann, B. Huber, C. Krüger and H. Schmidbaur, *Angew. Chem., Int. Ed.*, 1988, **27**, 1544.
- 4 (a) G. C. Bond, C. Louis and D. T. Thompson, *Catalysis by Gold*, Imperial College Press, London, 2006; (b) *Gold: Progress in Chemistry, Biochemistry and Technology*, ed. H. Schmidbaur, Wiley, Chichester, 1999.
- 5 (a) M. Haruta, *Catal. Today*, 1997, **36**, 153; (b) For a collection of recent reviews on gold chemistry and gold catalysis, see *Chem. Soc. Rev.*, 2008, issue 9.
- 6 (a) F. Furche, R. Ahlrichs, P. Weis, C. Jacob, S. Gilb, T. Bierweiler and M. M. Kappes, *J. Chem. Phys.*, 2002, **117**, 6982; (b) H. Häkkinen, B. Yoon, U. Landman, X. Li, H.-J. Zhai and L.-S. Wang, *J. Phys. Chem. A*, 2003, **107**, 6168.
- 7 S. Bulusu, X. Li, L.-S. Wang and X. C. Zeng, *Proc. Natl. Acad. Sci. U. S. A.*, 2006, **103**, 8326.
- 8 J. Li, X. Li, H.-J. Zhai and L.-S. Wang, *Science*, 2003, **299**, 864.
- 9 (a) I. L. Garzón, K. Michaelian, M. R. Beltrán, A. Posada-Amarillas, P. Ordejón, E. Artacho, D. Sánchez-Portal and J. M. Soler, *Phys. Rev. Lett.*, 1998, **81**, 1600; (b) H. Häkkinen, M. Moseler, O. Kostko, N. Morgner, M. A. Hoffmann and B. v. Issendorff, *Phys. Rev. Lett.*, 2004, **93**, 093401; (c) W. Huang, M. Ji, C.-D. Dong, X. Gu, L.-M. Wang, X. G. Gong and L.-S. Wang, *ACS Nano*, 2008, **2**, 897.
- 10 Y. Kondo and K. Takayanagi, *Science*, 2000, **289**, 606.
- 11 Y. Oshima, A. Onga and K. Takayanagi, *Phys. Rev. Lett.*, 2003, **91**, 205503.
- 12 J. Zhao, Q. Deng, A. Bachmatiuk, G. Sandeep, A. Popov, J. Eckert and M. H. Rümmeli, *Science*, 2014, **343**, 1228.
- 13 P. Koskinen and T. Korhonen, *Nanoscale*, 2015, **7**, 10140.
- 14 H. W. Kroto, J. R. Heath, S. C. O'Brien, R. F. Curl and R. E. Smalley, *Nature*, 1985, **318**, 162.
- 15 S. Iijima, *Nature*, 1991, **354**, 56.
- 16 K. S. Novoselov, A. K. Geim, S. V. Morozov, D. Jiang, Y. Zhang, S. V. Dubonos, I. V. Grigorieva and A. A. Firsov, *Science*, 2004, **306**, 666.
- 17 (a) T. Yokoyama, S. Yokoyama, T. Kamikado, Y. Okuno and S. Mashiko, *Nature*, 2001, **413**, 619; (b) B. Hulskens,

- R. Van Hameren, J. W. Gerritsen, T. Khouri, P. Thordarson, M. J. Crossley, A. E. Rowan, R. J. M. Nolte, J. A. A. W. Elemans and S. Speller, *Nat. Nanotechnol.*, 2007, **2**, 285; (c) V. Iancu and S.-W. Hla, *Proc. Natl. Acad. Sci. U. S. A.*, 2006, **103**, 13718; (d) Z. Shi and N. Lin, *J. Am. Chem. Soc.*, 2009, **131**, 5376; (e) S. Yoshimoto, E. Tsutsumi, Y. Honda, Y. Murata, M. Murata, K. Komatsu, O. Ito and K. Itaya, *Angew. Chem., Int. Ed.*, 2004, **43**, 3044.
- 18 C. T. White, D. H. Robertson and J. W. Mintmire, *Phys. Rev. B: Condens. Matter Mater. Phys.*, 1993, **47**, 5485.
- 19 J. P. Perdew, K. Burke and M. Ernzerhof, *Phys. Rev. Lett.*, 1996, **77**, 3865.
- 20 (a) P. Blöchl, *Phys. Rev. B: Condens. Matter Mater. Phys.*, 1994, **50**, 17953; (b) G. Kresse and D. Joubert, *Phys. Rev. B: Condens. Matter Mater. Phys.*, 1999, **59**, 1758.
- 21 G. Kresse and J. Hafner, *Phys. Rev. B: Condens. Matter Mater. Phys.*, 1993, **47**, 558.
- 22 (a) D. D. Koelling and B. N. Harmon, *J. Phys. C: Solid State Phys.*, 1977, **10**, 3107; (b) A. H. MacDonald, W. E. Pickett and D. D. Koelling, *J. Phys. C: Solid State Phys.*, 1980, **13**, 2675; (c) N. Takeuchi, C. T. Chan and K. M. Ho, *Phys. Rev. B: Condens. Matter Mater. Phys.*, 1989, **40**, 1565.
- 23 H. J. Monkhorst and J. D. Pack, *Phys. Rev. B: Condens. Matter Mater. Phys.*, 1976, **13**, 5188.
- 24 G. Kresse, J. Furthmüller and J. Hafner, *Europhys. Lett.*, 1995, **32**, 729.
- 25 S. J. Clark, M. D. Segall, C. J. Pickard, P. J. Hasnip, M. I. J. Probert, K. Refson and M. C. Payne, *Z. Kristallogr.*, 2005, **220**, 567.
- 26 G. J. Martyna, M. L. Klein and M. Tuckerman, *J. Chem. Phys.*, 1992, **97**, 2635.
- 27 A. R. Oganov and C. W. Glass, *J. Chem. Phys.*, 2006, **124**, 244704.
- 28 K. Momma and F. Izumi, *J. Appl. Crystallogr.*, 2011, **44**, 1272.
- 29 L.-M. Yang, E. Ganz, Z. Chen, Z.-X. Wang and P. v. R. Schleyer, *Angew. Chem., Int. Ed.*, 2015, **54**, 9468.
- 30 A. I. Boldyrev, J. Simons, X. Li and L. S. Wang, *J. Chem. Phys.*, 1999, **111**, 4993.
- 31 D. Y. Zubarev and A. I. Boldyrev, *J. Phys. Chem. A*, 2009, **113**, 866.
- 32 A. D. Becke and K. E. Edgecombe, *J. Chem. Phys.*, 1990, **92**, 5397.
- 33 A. Savin, O. Jepsen, J. Flad, O. K. Andersen, H. Preuss and H. G. von Schnerring, *Angew. Chem., Int. Ed.*, 1992, **31**, 187.
- 34 B. Silvi and A. Savin, *Nature*, 1994, **371**, 683.
- 35 (a) L.-M. Yang, V. Bačić, I. A. Popov, A. I. Boldyrev, T. Heine, T. Frauenheim and E. Ganz, *J. Am. Chem. Soc.*, 2015, **137**, 2757; (b) L.-M. Yang, I. A. Popov, A. I. Boldyrev, T. Heine, T. Frauenheim and E. Ganz, *Phys. Chem. Chem. Phys.*, 2015, **17**, 17545; (c) L.-M. Yang, I. A. Popov, T. Frauenheim, A. I. Boldyrev, T. Heine, V. Bačić and E. Ganz, *Phys. Chem. Chem. Phys.*, 2015, DOI: 10.1039/c5cp04893a.
- 36 L.-M. Yang, T. Frauenheim and E. Ganz, *Phys. Chem. Chem. Phys.*, 2015, **17**, 19695.